Preprint of article about an open hardware RTU device.

Multiple Sensor Interface by the same hardware to USB and serial connection

David Nuno Quelhas *
Preprint submitted to 'arXiv', April 10, 2022

Abstract

The Multiple Sensor Interface is a simple sensor interface that works with USB, RS485 and GPIO. It allows one to make measurements using a variety of sensors based on the change of inductance, resistance, capacitance, and frequency using the same connector and same electronic interface circuit between the sensor and the microcontroller. The same device also provides some additional connectors for small voltage measurement. Any sensors used for the measurement of distinct phenomena can be used if the sensor output is based on inductance, resistance, capacitance or frequency within the measurement range of the device, obtaining a variable precision depending on the used sensor. The device presented is not meant for precise or accurate measurements. It is meant to be a reusable hardware that can be adapted/configured to a varied number of distinct situations, providing, to the user, more freedom in sensor selection as well as more options for device/system maintenance or reuse.

Keywords: Sensor systems and applications; Oscillators; Design aiming for reuse, repurpose, repair, customization.

1 Introduction

The electronic waste (e-waste) is a modern problem under increasing concern and awareness, there are various possible approaches to reduce and mitigate it, the most obvious is the collection and recycling of discarded devices, however the most ideal is just to make technology that lasts because not only is physically fit by quality design, production, and components; but because its design was intended to be most versatile ensuring the same device can be used and reused in various applications/contexts just by changing connections, jumpers, and firmware configurations. Some design aspects for making a device more reusable are: the use of standard connectors and protocols, think of it as a module to be part of a larger system, minimize barriers for connecting/interfacing components and devices from distinct manufacturers.

1.1 Project objectives and trade-offs

This article is focused on the design of a sensor interface device with USB and serial(UART,RS-485), aimed to allow the interface to many distinct 2-wire sensors based on the change of inductance, resistance, capacitance, frequency, and also small voltage; sensors that can be interchanged using the same hardware and same port of the device, thus meaning the electronics designed must also be versatile.

Obviously providing a versatile device to the users will have its negative trade-offs, like:
1- probably significant lower precision/accuracy;
2- some sensor calibration must be provided/done by the end user after replacing a sensor;
3- the calibration function will not be linear or 'easy' as desired for sensors and its interfaces.

However, for some applications the mentioned trade-offs are not necessarily a deal-breaker, like when the user is technical and is ok with using a device that requires more setup/configuration, some users like devices that are more customizable or repairable. Also is possibly valued a device that if no longer useful for a user, it might still be useful for another user on a different application/context.

1.2 License and context

The hardware design here disclosed is distributed under "CERN Open Hardware Licence Version 2 - Weakly Reciprocal" (CERN-OHL-W), its associated software/firmware under GNU licenses (GPL, LGPL).

This article is about a 'hobby' project done by the author (David Nuno Quelhas, MSc Electronics Eng, alumni of Instituto Superior Tecnico, Portugal) with occasional 'work' between the years 2012 and 2021 on his 'free time'.

1.3 Prior art review

The topic and devices commonly described in literature as 'Multiple Sensor Interface' and also as 'Universal Sensor Interface', commonly fall under 3 distinct categories: a) Device that has a more versatile interface or signal conditioning circuit capable of interfacing various sensor types; b) Device that includes various specialized interfaces or signal conditioning circuits for each sensor type, typically built using various PCB boards for the sensors, to connect or stack into a PCB board with a micro-processor that will register and/or transmit the measurements, or alternatively have all these different circuits integrated inside a single integrated circuit (micro-chip); c) Hardware and/or software systems that collect or register sensor data from various distinct sensing devices/circuits, that may apply some processing to the raw data for obtaining measurements, then to be transmitted to other systems or to a data storage, and so these hardware/software systems may also be called/named 'interface'.

*Lisboa, Portugal; E-mail: david.n.quelhas@gmail.com
https://pt.linkedin.com/in/dquelhas
ORCID: 0000-0002-0282-0972
https://multiple-sensor-interface.blogspot.com

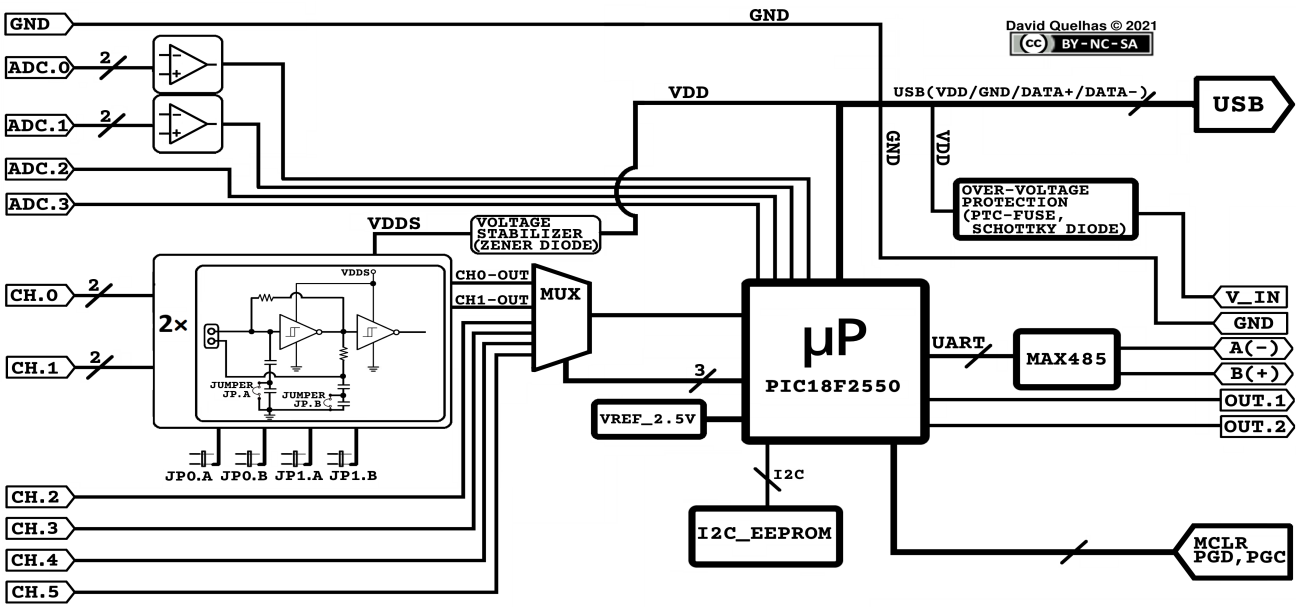

Figure 1: Diagram of the Multiple Sensor Interface device.

The article review presented here will be about 'more versatile interface or signal conditioning circuit' that is the category most similar to this article. Types of versatile sensor interface found on prior art:

1- Interfacing resistive or capacitive sensors by measuring the charge-discharge time of an RC circuit, or measuring the frequency or PWM from an oscillator whose pace is controlled by the speed of a capacitor charge-discharge trough a resistor; for example: [6], [7], [8] .

2- Interfacing sensors based on the variation of impedance (includes sensor based on variation of resistance, capacitance or inductance) by an LCR meter, impedance meter, or potentiostat circuit; for example: [9], [10], [11], [12] .

The Multiple Sensor Interface presented on this article has a working principle more similar to the circuits mentioned as type 1 (RC time or frequency or PWM of oscillator), however in comparison with the mentioned references/articles, the interface circuit of this article can interface more distinct sensor types, namely besides interfacing resistive and capacitive sensors it also interfaces inductive sensors and sensors by frequency measurement using exactly the same circuit and connector/port, also it is a simple circuit with a reduced number of components.

The Multiple Sensor Interface presented on this article in comparison to the circuits mentioned as type 2 (LCR or impedance meters), has the advantage of not requiring an AC voltage/signal generator for exciting the measurement circuit, and not requiring the complex hardware and/or complex post processing for digitizing voltage signal waveforms, that is typically required for the calculation of amplitude and phase difference of voltage signals, on the measurement of impedance by LCR or impedance meters.

A comparison regarding the accuracy or precision of this sensor interface and other interfaces/devices was not made, since the stated focus of the article is how to achieve a most versatile sensor interface, and also considering that such comparison may be easier when considering specific type(s) of sensor/application.

2 Design, Materials and Methods

2.1 Sensor Interface Device

Here is presented the Multiple Sensor Interface (Fig.1), the interface main components / sub-circuits are: The connectors and sensor interface circuits (oscillators) for inductance, resistance, capacitance, and frequency (CH.0, CH.1); the connectors and over-voltage protection(zener diode) for frequency measurement (CH.2, CH.3, CH.4, CH.5); the connectors and interface circuit for voltage measurement (ADC.0, ADC.1, ADC.2, ADC.3); analog multiplexer for the sensor channels, the microprocessor(PIC18F2550); I2C EEPROM for storing calibration tables; USB connector; connector and circuit for RS-485 and UART; digital outputs connector (OUT.1, OUT.2).

The digital outputs have the value of a boolean function defined by the user, boolean functions with logic variables that are the result of a comparison ('bigger' or 'smaller' than), between the value/measurement of a sensor channel and a configurable threshold value. The connectors used for frequency measurement may be connected to external single sensor interface circuits (oscillators).

2.2 The sensor interface circuit (oscillator)

The sensor interface (Fig.2) is an oscillator with a circuit design based on the Pierce oscillator with some modifications. The 1st difference is that there is no quartz crystal, and on the location of the crystal will be connected the sensor to be measured (variable inductance or resistance or capacitance), the 2nd difference is that instead of simple inverters ('NOT' gates) will be used Schmitt-trigger inverters(high-speed Si-gate CMOS, 74HC14), this is a very relevant difference that will allow the oscillator to work even with a resistive or capacitive sensor, in fact the interface circuit works with sensors mostly as a Schmmit-Trigger oscillator. Also the Schmitt-Trigger inverters may minimize signal jitter of the oscillator output.

The sensor interface circuit has 2 pairs of series capacitors (C1 2.2nF,C1-A 22pF and C2 2.2nF,C2-B 22pF) instead of just 2 capacitors(C1,C2) so the value of C1 and C2

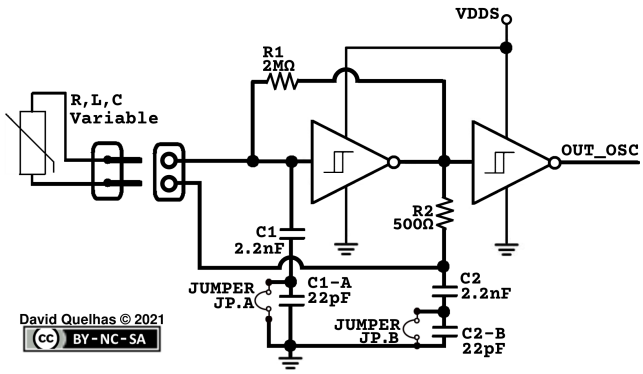

Figure 2: Schematic of the sensor interface circuit (oscillator).

can be adjusted just by placing/removing a jumper; placing a jumper removes C1-A or C1-B from the circuit making 2.2nF the value of C1 or C2; removing the jumper lets the capacitors in series making 21.78pF the total value of (C1, C1-A) or (C2, C2-B). So on the rest of the article, whenever is mentioned C1 or C2 is meant the resulting capacitor value that can be 2.2nF(jumper on) or 21.78pF(jumper off), accordingly with mentioned jumper configuration.

The sensors can be connected directly on the Multiple-Sensor Interface(on the screw terminals/connectors), or by using a cable; for a cable longer than 20cm is recommended the use of shielded twisted-pair(STP) cable to prevent cross-talk between sensor channels or external EMI.

2.3 Measurement process

The Multiple-Sensor device has a microprocessor (PIC18F2550) that is able to make frequency and voltage measurements, so the device makes frequency measurements for sensor channels CH.0 to CH.5 ; and makes voltage measurements for sensor channels ADC.0 to ADC.3; these frequency and voltage measurements made by the device are designated as the RAW_value of a sensor channel. To obtain the measurement of a sensor channel, the device uses a 2 column calibration table, that is a long list of points (RAW_value; measurement) relating the measurement value (obtained during calibration by an external reference device) to the corresponding RAW_value obtained on the Multiple-Sensor device, these calibration tables are stored on an I2C EEPROM memory on the Multiple-Sensor device.

The Multiple-Sensor device can work in two modes: single-channel or multiple-channel, the CH.0 to CH.5 RAW_value(frequency) are calculated through a counter/timer of the PIC18F2550 by periodically reading its value and calculating the frequency f=count/period ([Hz]=[cycles]/[s]). So in single-channel mode the frequency is always calculated on the selected/enabled sensor channel, in multiple-channel mode the frequency is calculated for each sensor channel sequentially (time-division multiplexing), since there are 6 channels to measure but only on counter/timer of the microprocessor for that job. Thus in multiple-ch mode a measurement takes 6x more time to be updated/refreshed than in single-ch mode.

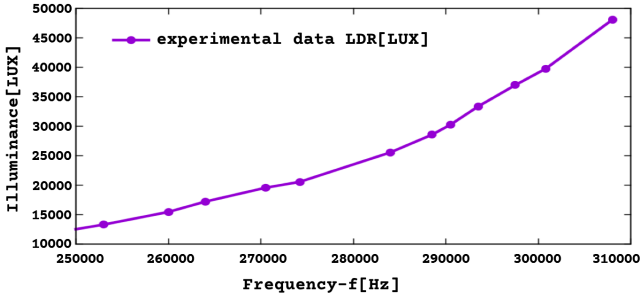

Figure 3: Plot experimental data with line, LDR light(brightness) sensor connected on Multiple-Sensor Interface; example of a calibration table exclusively from experimental data.

For the sensor channels ADC.0 to ADC.3 the RAW_value is the voltage of those channels measured by using the ADC (Analog to Digital Converter) of the microprocessor and also reading a 2.5V voltage reference.

The sensor measurements are calculated by searching the RAW_value on the correspondent calibration table, and by using from the table 2 points (RAW_value,measurement) referenced here as points P and Q such that the measured RAW_value is bigger than RAW_value of P and is lower than RAW_value of Q; then is calculated a linear equation: $measurement = a \cdot (\text{RAW\_value}) + b$, defined by the points P and Q. So every-time the device calculates a sensor measurement, it will calculate the correspondent linear equation for the current RAW_value and use it to obtain the current measurement (Fig.3) .

2.4 Device calibration for a sensor

Device calibration is about obtaining calibration tables for each sensor channel, here are 2 ways to obtain it:

1- Do a full manual calibration using an external meter as reference where both the reference meter and the Multiple-Sensor device(with a sensor connected) are exposed to same stimulus/environment that is controllable by the user to produce all adequate variations/intensities necessary to record an extensive calibration table, with all experimental pairs of (RAW_value,measurement).

2- Using a known function that relates the measured phenomena to the obtained RAW_value on the Multiple-Sensor device (obtained by theoretical or experimental study), although a purely theoretical calibration could be used, probably is better or easier to obtain a calibration table by using a known function and have its constants/parameters calculated by a data fitting to some few experimental data points (RAW_value, measurement) obtained for the device calibration. So for example if the known function had 6 constants/parameters, you would require at least 6 different experimental measurements to obtain the function for that sensor channel, then having the function is just a question calculating a longer list of pairs (RAW_value,measurement) on the desired measurement range. Fig.4 is the result of fitting the model function $Illuminance(f) = (a + (b/(c + d \cdot f))) \cdot ((n \cdot f^2) + m)$, to the points (229Hz, 0LUX; 8500Hz, 10LUX; 14000Hz, 30LUX; 76500Hz, 300LUX; 130000Hz, 1072LUX; 194000Hz, 3950LUX).

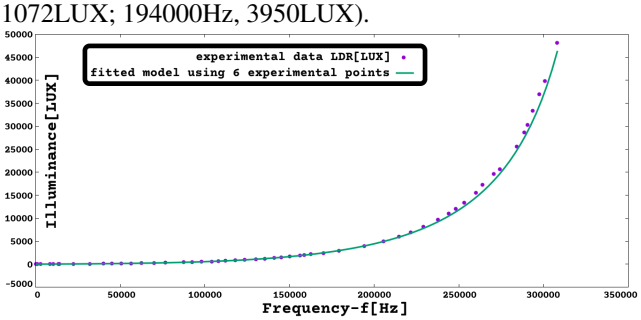

Figure 4: Plot experimental data and fitted model(by using 6 points), LDR light(brightness) sensor connected on Multiple-Sensor Interface.

3 Results and Analysis

3.1 Device testing

The author developed and built prototypes of the described device, made of the components described on the previous section and on Fig.1 diagram. Then the device was experimented with various different sensors; including various common sensor components, namely: LDR (Light Dependent Resistor or also designated as photo-resistor), RTD(Resistance Temperature Detector), FSR(Force Sensitive Resistor), Relative-Humidity sensor (RH to impedance); as well some handmade sensors done by the author for the purpose of exploring the device usability, namely: a water level sensor (by variation of capacitance based on water height), a proximity sensor (based on the variation of inductance of a flat coil, caused by the vicinity of a metallic object, or the vicinity of a non-metallic object covered with aluminum or copper adhesive tape), a force sensor (based on resistance variation when pressed) made using 'carbon impregnated foam' (also known as ESD/antistatic foam), aluminum foil and adhesive tape.

The tests done with the device connected on the various mentioned sensors, were made with the purpose of verifying that the device is indeed usable with various types of sensors, but those tests are not the most appropriate for studying how the device works, or for characterizing the device itself by determining its usability range, or for gathering quantitative data about the device to be used along with the data from a sensor datasheet for determining its compatibility.

So the tests chosen for characterizing the device were records (on 2 column tables) of the measured values of inductance, resistance, capacitance paired with measured frequency on the Multiple Sensor Interface device. For these tests (Fig.5) were used arrays(PCBs) of inductors, resistors, capacitors that allow to obtain various different values just by changing a jumper/switch, also were used single components (including in series or parallel association); these fixed value components were connected as the sensor on the device.

The various figures with plots/graphs on this article will show both the experimental data obtained on the mentioned tests, as well the theoretical graphs obtained from circuit analysis of the device, for comparison purposes; also at the end of the article on Appendix A are tables with the experimental data obtained on the mentioned tests.

Figure 5: Equipment used for testing; R, C, L test components (top); and the Multiple-Sensor Interface (center bottom).

3.2 Sensor Interface Circuit Analysis

3.2.1 Multiple-Sensor Interface for Inductive sensors

When is connected an inductor or inductive sensor the Multiple-Sensor Interface (Fig.2) may work as a Pierce Oscillator(where the sensor is connected instead of a quartz crystal). The theoretical analysis used here for the oscillator was based on a model of 2 circuit blocks named 'A' and 'β' connected for feedback by connecting the output of one to the input other. The 'A' is an electronic amplifier providing voltage gain, the 'β' is an electronic filter providing frequency selection (resonance), so whatever voltage signal amplified by 'A' is frequency selected by 'β' and feed back to the input of A for further amplification. As known, this oscillator is start-up by whatever noise (v_s) available at the input of 'A', Fig.6 is a diagram depicting this concept.

The analysis of the circuit as Pierce oscillator was made using the Barkhausen stability criterion, that says $A\beta = 1$ to be possible to occur sustained oscillations (oscillations on steady state analysis). The purpose/focus is to obtain the inductance(of sensor) as function of oscillation frequency, although most of the circuit analysis strategy used here is similar as for typical Pierce Oscillator with piezoelectric crystal, as available on the bibliography list "Crystal Oscillators for Digital Electronics" class notes by Peter McLean [2]. So from $A\beta$=1 results: $|A\beta|$=1 and $\angle A\beta = \pm n2\pi$. This mathematical expression simply says that a circuit with a feedback loop after reaching the steady-state is expected that any voltage signal (for example V_o) will remain steady.

Starting the analysis on Fig.7, using a possible representation of Fig.6 diagram with the 'feedback network' represented by its hybrid parameters (2-port network h-parameters) [1], [2] .

The Schmitt-Trigger inverter and resistors R_1, R_2 belong to block 'A', the capacitors C_1, C_2, and inductive sensor L_s belong to block 'β'.

Since the 'Basic Amplifier' has a very big input resistance the current I_1 will be very small (the electric current

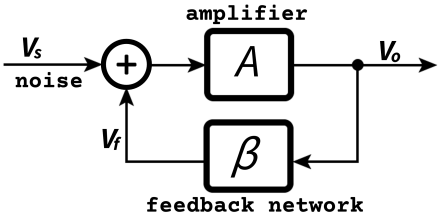

Figure 6: Diagram of model for the oscillator with an inductive sensor (Pierce Osc., model of feedback linear oscillator).

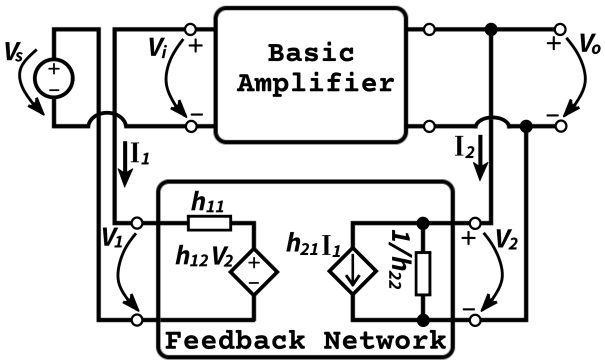

Figure 7: Representation of oscillator circuit by the h-parameters for feedback circuit (Pierce Osc.).

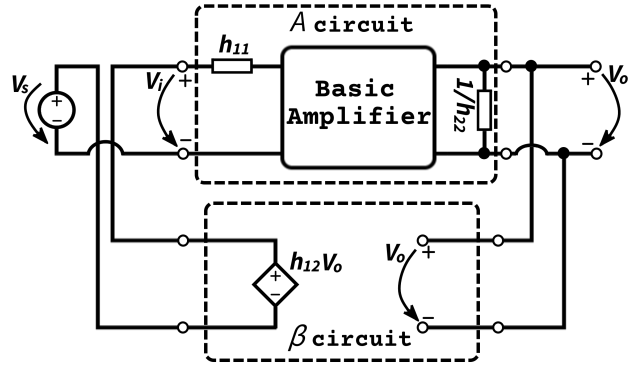

Figure 8: Simplified representation of oscillator circuit (Pierce osc.)

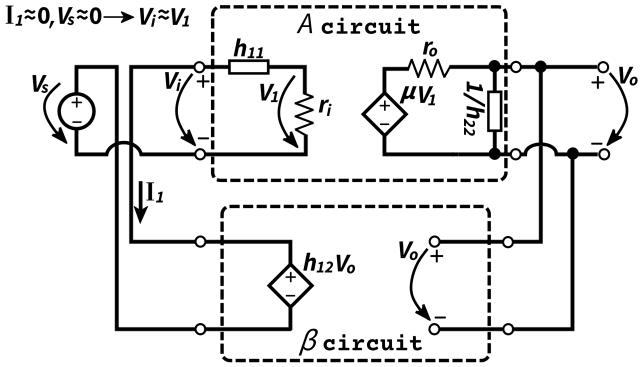

Figure 9: More simplified representation of the circuit (Pierce osc.)

on the input of the inverter, CMOS 'NOT' gate, is negligible), so by using the h-parameters to represent the feedback circuit block is possible to make the following simplifications/approximations: 1- The current source $h_{21}I_1$ is also negligible (equal to zero, so removed from circuit); 2- The voltage drop across component h_{11} is negligible (since $V_{11} = h_{11}I_1$, $I_1 \to 0 \Rightarrow V_{11} \to 0$) and so h_{11} can be relocated to inside the circuit block 'A' keeping V_i as the name for the voltage drop on the input of 'A' block; 3- The $1/h_{22}$ can be relocated to inside the circuit block 'A' since is connected in parallel to the input of 'β' block that is also the output of 'A' block [2] .

The block 'Basic Amplifier' is then replaced by its Thevenin equivalent circuit, obtaining Fig.9 circuit. From this is obtained the transfer function (Laplace transform) of 'A' block (V_o=AV_i , $1/h_{22}$=h_{22}^{-1}) and 'β' block (V_1=βV_2):

$$A = \frac{h_{22}^{-1}}{h_{22}^{-1}+r_o}\mu\frac{r_i}{r_i+h_{11}} \qquad\qquad \beta = h_{12}$$

The feedback network (the same network displayed on Fig.7 represented by h-parameters) is the frequency-selecting π(shaped)-network on Fig.10, where Z_1, Z_2, Z_s are respectively C_1,C_2,L_{sensor} of the Multiple Sensor Interface with an inductive sensor (Pierce oscillator).

Based on the circuit of the feedback network and using the definitions of h-parameters of a 2-port network are obtained the values:

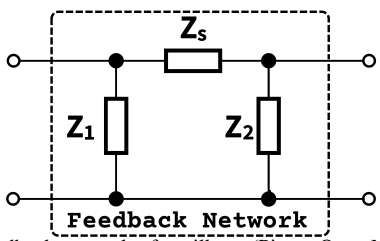

Figure 10: Feedback network of oscillator (Pierce Osc., Multiple-Sensor Int. with inductive sensor).

$h_{11} = Z_1||Z_s \qquad h_{22}^{-1} = Z_2||(Z_1+Z_s) \qquad h_{12} = \frac{Z_1}{Z_1+Z_s}$

(where $||$ is the impedance of 2 components in parallel, $Z_1||Z_s = (Z_1Z_s)/(Z_1+Z_s)$; $h_{11} = (V_1/I_1)|_{V_2=0}$; $h_{12} = (V_1/V_2)|_{I_1=0}$; $h_{22} = (I_2/V_2)|_{I_1=0}$) [1] .

Finally:

A=$\frac{Z_2||(Z_1+Z_s)}{Z_2||(Z_1+Z_s)+r_o}\mu\frac{r_i}{r_i+(Z_1||Z_s)}$ $\qquad$ β=$\frac{Z_1}{Z_1+Z_s}$

In the circuit of Pierce oscillator (Fig.2) the amplifier was made by a gate inverter (CMOS 'NOT' gate) and a feedback resistor (R_1=$2M\Omega$), biasing the inverter and allowing it to function as a high-gain inverting amplifier. The input resistance of CMOS 'NOT' gate is very large and so making the approximation r_i=$+\infty$ the expression of 'A' is significantly simplified, So obtaining [2] :

$$A\beta = \left(\frac{Z_2||(Z_1+Z_s)}{Z_2||(Z_1+Z_s)+r_o}\mu\right)\left(\frac{Z_1}{Z_1+Z_s}\right) = \frac{Z_1Z_2\mu}{Z_2(Z_1+Z_s)+r_o(Z_1+Z_2+Z_s)} \quad (1)$$

If Z_1, Z_2, Z_s are purely reactive impedances given by Z_1=jX_1, Z_2=jX_2, Z_s=jX_s (j=$\sqrt{-1}$), then (1) becomes:

$$A\beta = \frac{X_1X_2\mu}{X_2(X_1+X_s) - jr_o(X_1+X_2+X_s)} \quad (2)$$

The Barkhausen criterion states $A\beta$=$1 \to \angle A\beta$=$\pm n2\pi$, this means the phase shift of the loop '$A\beta$' must be zero, and so that implies that the imaginary part of (2) must be zero. That is, for stable oscillations on the circuit of Fig.7 with a Feedback Network of Fig.10, it must be assured [2] :

$$X_1(\omega_0) + X_2(\omega_0) + X_s(\omega_0) = 0 \quad (3)$$

At the frequency ω_0 (frequency of oscillation at steady state), using (3) with (2), is obtained [2] :

$$A(\omega_0)\beta(\omega_0) = -\mu\frac{X_1(\omega_0)}{X_2(\omega_0)} \quad (4)$$

To start the oscillations the loop gain must be grater than unity (during Transient Response), but after achieving the Steady State Response on the Pierce oscillator for oscillations to occur the loop gain $A(\omega_0)\beta(\omega_0)$ of (4) must be equal to '1'(unity). Since the amplifier is an inverter ('NOT' gate with R_1 feedback resistor) then μ is a negative number, and so $X_1(\omega_0)$ and $X_2(\omega_0)$ must have the same sign (both positive or negative).

Thus, if $Z_1(\omega_0)$ is capacitive($X_1(\omega_0) = -1/(\omega_0C_1)$), then by (4) $Z_2(\omega_0)$ must also be capacitive ($(X_2(\omega_0) = -1/(\omega_0C_2))$ [2] .

Considering this and using (3) its possible to conclude that $Z_s(\omega_0)$ must be inductive since $X_s(\omega_0) = -X_1(\omega_0) - X_2(\omega_0)$, this is if $X_1(\omega_0)$ and $X_2(\omega_0)$ are negative numbers then $X_s(\omega_0)$ must be a positive number, then $X_s = \omega_0L_s$.

So having C_1, C_2, L_s on the feedback network (where L_s is the component representing the inductive sensor on the Multipl-Sensor Interface) the (3) becomes:

$$-\frac{1}{\omega_0C_1} - \frac{1}{\omega_0C_2} + \omega_0L_s = 0 \quad (5)$$

So defining "load capacitance" C_L as [2] :

$$\frac{1}{C_L} = \frac{1}{C_1} + \frac{1}{C_2} \quad (6)$$

The frequency of oscilation on the Pierce oscillator (using C_1, C_2, L_s) is:

$$\omega_0 = \frac{1}{\sqrt{L_s C_L}} \quad \Leftrightarrow \quad f_0 = \frac{1}{2\pi\sqrt{L_s C_L}} \tag{7}$$

So the expression (theoretical) of measured inductance L_{sensor} as a function of frequency(f) is:

$$L_{sensor} = L_s = \frac{1}{4\pi^2 C_L f^2} = \frac{C_1 + C_2}{4\pi^2 C_1 C_2 f^2} \tag{8}$$

On experimental tests done was observed that when using C_1=C_2=2.2nF (JP.A and JP.B closed) or when using C_1=21.78pF (JP.A open), C_2=2.2nF (JP.B closed), with decreasing values of L_s connected, the oscillation frequency exhibited a sudden change, at some small value of L(around $10\mu H$ for C_1=C_2=2.2nF), not coherent with theoretical model of Pierce oscillator. This may be related to the fact that the same circuit also implements a Schmitt-Trigger oscillator(next section), that oscillates under different criteria, so the author opinion is when L_s approaches some small value it may change from Pierce oscillator to Schmitt-Trigger oscillator. Fig.11 and Fig.12 shows the experimental data for various inductance values connected as the sensor and the plot $L_s(f)$ using (8) with C_1=C_2=2.2nF and C_1=21.78pF, C_2=2.2nF.

Since the mentioned sudden change of oscillator mode and frequency is not adequate on a $L_s(f)$ function usable for sensor interfacing; then on experimental tests with jumper configuration: JP.A on and JP.B off (C_1=$2.2nF$, C_2=21.78pF), it was observed a continuous and progressive $f(L_s)$ function. With C_1=2.2nF, C_2=21.78pF, the experimental $L_{s,expr}(f)$ followed a straight line for L_s in $[0\mu H; 100\mu H]$, then for L_s>$100\mu H$ the experimental $L_{s,expr}(f)$ continued with a shape that has some visual similarity to theoretical (as Pierce oscillator), but with significantly different L_s values. It was noticed that for larger values of L_s the theoretical (Pierce oscillator, JP.A on, JP.B off) could be approximated to the experimental data by a constant multiplicative factor ($L_{s,expr}(f) \approx 0.03 \cdot L_{s,theo}(f)$, for L_s>1mH), as visible in Fig.13.

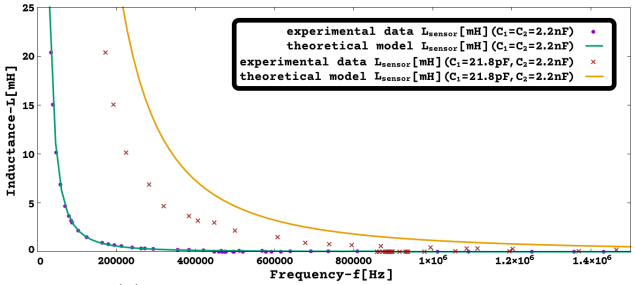

Figure 11: $L_s(f)$[mH]([Hz]) with C_1=C_2=2.2nF and C_1=21.78pF, C_2=2.2nF (Pierce Osc., Multi-Sensor Int. with inductive sensor)

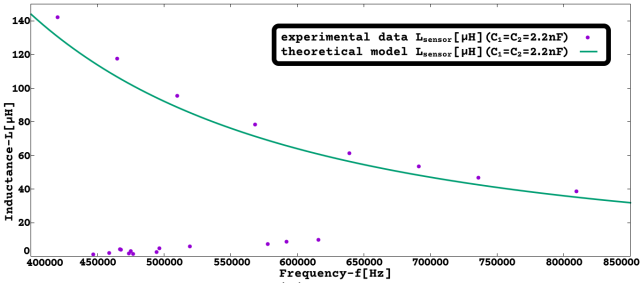

Figure 12: Frequency jump of $L_s(f)[\mu H]([Hz])$ with C_1=C_2=2.2nF (Pierce Osc., Multi-Sensor Int. with inductive sensor).

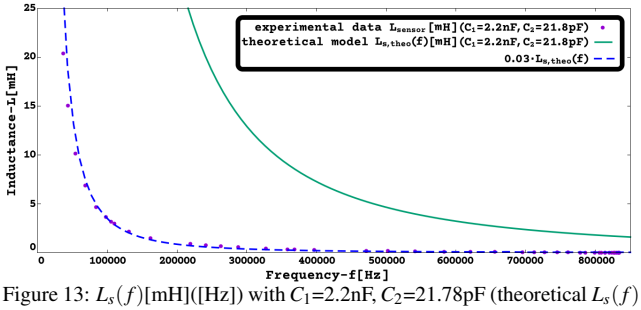

Figure 13: $L_s(f)$[mH]([Hz]) with C_1=2.2nF, C_2=21.78pF (theoretical $L_s(f)$ as a Pierce Osc.).

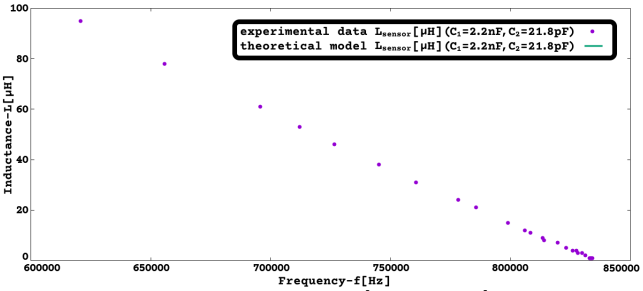

Figure 14: Experimental data of L_s in $[0\mu H; 100\mu H]$, with C_1=2.2nF, C_2=21.78pF (theoretical $L_s(f)$ as a Pierce Osc.).

For modeling(data fitting) purposes, the author knows that a function $L_s(f)$=$(a+(b/(c+d\cdot f)))\cdot(n\cdot f+m)$, where 'a,b,c,d,m,n' are constants to fit, can be fitted to experimental data on both low and high values of L_s.

On following section 3.3 was used an approximated model (for Schmitt-Trigger oscillator) applied to Multiple-Sensor Interface with inductive sensor (JP.A on, JP.B off), that exhibited a theoretical $L_s(f)$ plot much closer to the experimental data, corroborating the hypothesis that with jumper configuration JP.A on, JP.B off (C_1=2.2nF, C_2=21.78pF), it operates as a Schmitt-Trigger oscillator, where L_s acts as an impedance influencing C_1 charge and discharge speed.

3.2.2 *Multiple-Sensor Interface for Resistive sensors*

In case you connect a resistive sensor (or capacitive) to the Multiple-Sensor Interface it will not be able to satisfy the conditions for oscillation of equations (3) and (4), consequent of the Barkhausen criterion applied to the circuit, as it was explained on the previous section that on the π(shaped)-network of Fig.10 if Z_1 and Z_2 are capacitive (corresponding to C_1 and C_2) then Z_s must be inductive so that $A(\omega_0)\beta(\omega_0)$=1. So the conclusion is when you connect a resistive sensor (or capacitive) you no longer have a Pierce Oscillator. The Multiple-Sensor Interface is made using Schmitt-trigger inverters(high-speed Si-gate CMOS, 74HC14), and the Schmitt trigger is a bistable multivibrator that can be used to implement another type of multivibrator, the relaxation oscillator. So in the case of a resistive sensor the circuit to analyze is a Schmitt-trigger inverter connected to a network of resistors and capacitors.

To analyze this circuit the Schmitt-Trigger inverter was replaced by a theoretical switch that changes the voltage of node v_o to VDDS (power supply stabilized voltage for the sensor interface) when voltage v_i is lower than V_T^-, and changes v_o to GND when voltage v_i is higher than V_T^+.

- So the circuit of Fig.15 was analyzed to obtain $f(R_s)$, and then its inverse function $R_s(f)$=R_{sensor} that may be useful for using/configuring the Multiple-Sensor Interface. Notice that i_i≈0 since v_i is the input of a Schmitt-trigger in-

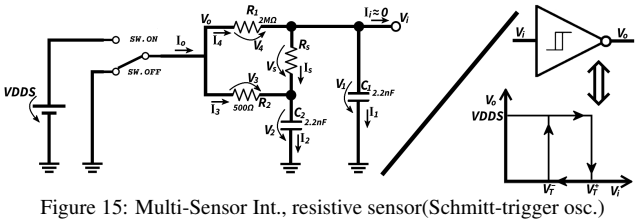

Figure 15: Multi-Sensor Int., resistive sensor(Schmitt-trigger osc.)

verter (high-speed Si-gate CMOS) that has a very high input impedance and so $i_i \approx 0$ is an appropriate approximation simplifying the circuit. So from the circuit are obtained the equations:

Nodes and loops: $i_4 = i_s + i_1$, $i_3 + i_s = i_2$, $i_o = i_3 + i_4$, $i_1 + i_2 = i_o$, $i_1 + i_2 = i_3 + i_4$, $v_1 - v_2 - v_s = 0$, $v_4 + v_s + v_2 - v_o = 0$, $v_4 + v_s - v_3 = 0$, $v_3 = v_o - v_2$, $v_4 = v_o - v_i$, $v_2 = v_i - v_s$.

Components: $i_1 = C_1(dv_1/dt)$, $i_2 = C_2(dv_2/dt)$, $v_3 = R_2 i_3$, $v_4 = R_1 i_4$, $v_s = R_s i_s$.

Solving:

$$\frac{v_o - v_i}{R_1} = \frac{v_s}{R_s} + C_1 \frac{dv_i}{dt} \tag{9}$$

$$\frac{v_o - v_i + v_s}{R_2} + \frac{v_s}{R_s} = C_2 \frac{dv_2}{dt} \tag{10}$$

Solving: $v_2 = v_i - v_s \Rightarrow dv_2/dt = d(v_i - v_s)/dt \Rightarrow dv_2/dt = (dv_i/dt) - (dv_s/dt)$

So using the previous result the (10) can be changed to:

$$\frac{v_o - v_i}{R_2} + \left(\frac{1}{R_2} + \frac{1}{R_s}\right) v_s = C_2 \left(\frac{dv_i}{dt} - \frac{v_s}{dt}\right) \tag{11}$$

Solving (9) for v_s is obtained:

$$v_s = \frac{R_s(v_o - v_i)}{R_1} - R_s C_1 \frac{dv_i}{dt} \tag{12}$$

Calculating the derivative on both sides of (12) is obtained (remember v_o is a constant equal to VDDS or GND depending on the position of the switch 'SW'):

$$\frac{dv_s}{dt} = \frac{-R_s}{R_1}\frac{dv_i}{dt} - R_s C_1 \frac{d^2 v_i}{dt^2} \tag{13}$$

Now using (12) and (13) to remove the variables v_s and dv_s/dt from equation (11) is obtained an equation solvable for determining $v_i(t)$:

$$\left(\frac{1}{R_2} + \frac{R_s}{R_2 R_1} + \frac{1}{R_1}\right)(v_o - v_i) = \left(C_1\left(1 + \frac{R_s}{R_2}\right) + C_2\left(1 + \frac{R_s}{R_1}\right)\right)\frac{dv_i}{dt} + R_s C_1 C_2 \frac{d^2 v_i}{dt^2} \tag{14}$$

The equation (14) is of the type: $c(v_o - v_i) = b(dv_i/dt) + a(d^2 v_i/dt^2)$ that has the general solution: $v_i(t) = v_o + k_1 e^{\lambda_1 t} + k_2 e^{\lambda_2 t}$, where k_1,k_2 are integration constants to be defined by 'initial conditions' and λ_1, λ_2 are defined by: $a\lambda^2 + b\lambda + c = 0 \Leftrightarrow \lambda = \frac{-b \pm \sqrt{b^2 - 4ac}}{2a}$ and e is the Euler-Napier constant $e = \sum_{n=0}^{\infty}(1/(n!))$.

So for a solution to this circuit: $a = R_s C_1 C_2$,
$b = (C_1(1 + (R_s/R_2))) + (C_2(1 + (R_s/R_1)))$,
$c = (1/R_2) + (R_s/(R_2 R_1)) + (1/R_1)$.

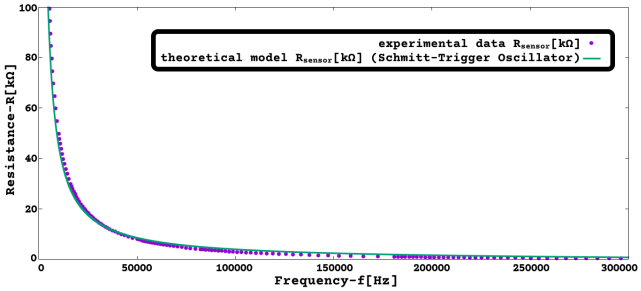

Figure 16: R_s[kΩ] versus frequency[0Hz, 300kHz] (Schmitt-Trigger Oscillator, Multiple-Sensor Interface with resistive sensor).

Is selected the solution $\lambda_2 = \frac{-b + \sqrt{b^2 - 4ac}}{2a}$ by setting k_1=0, because is the one that provides an adequate value for $v_i(t)$, $f(R_s)$, consistent with experimental data, however for obtaining the function $R_s(f)$ you may use any.

For convenience of making $v_i(t)$ more similar to typical RC circuits is defined $\tau = -1/\lambda$, and so $v_i(t) = v_o + k_2 e^{-t/\tau_2}$.

Charging time of C_1: $v_o = VDDS$
$v_i(t{=}0) = V_T^- \rightarrow V_T^- = VDDS + k_2 e^0 \rightarrow k_2 = V_T^- - VDDS$
$v_i(t{=}T_C) = V_T^+ \rightarrow V_T^+ = VDDS + k_2 e^{-T_C/\tau_2} \rightarrow$
$\rightarrow \quad T_C = -\tau_2 ln((V_T^+ - VDDS)/(V_T^- - VDDS))$

Discharging time of C_1: $v_o = 0$
$v_i(t{=}0) = V_T^+ \rightarrow V_T^+ = 0 + k_2 e^0 \quad \rightarrow \quad k_2 = V_T^+$
$v_i(t{=}T_D) = V_T^- \rightarrow V_T^- = 0 + k_2 e^{-T_D/\tau_2} \rightarrow$
$\rightarrow \quad T_D = -\tau_2 ln(V_T^-/V_T^+)$

The time for a complete cycle of charge and discharge of C_1 is: $T = T_C + T_D$; the frequency of $v_i(t)$ is $f = 1/T$.

Solving: $T = -\tau_2 \left(ln\left(\frac{V_T^+ - VDDS}{V_T^- - VDDS}\right) + ln\left(\frac{V_T^-}{V_T^+}\right)\right) \Leftrightarrow$
$T = \tau_2 ln\left(\frac{(V_T^- - VDDS)V_T^+}{(V_T^+ - VDDS)V_T^-}\right)$

For convenience defining the constant 'H' by:

$$H = ln\left(\frac{(V_T^- - VDDS)V_T^+}{(V_T^+ - VDDS)V_T^-}\right),$$

then $f = 1/T \Leftrightarrow f = 1/(\tau_2 H) \Leftrightarrow f = -\lambda_2/H$.

So the expression (theoretical) of measured resistance R_{sensor} as a function of frequency(f) is:

$$R_{sensor} = R_s = \frac{(C_1 + C_2)R_2 R_1 H f - R_2 - R_1}{(C_2 R_2 H f - 1)(C_1 R_1 H f - 1)} \tag{15}$$

Using the values C_1=C_2=2.2nF, R_2=500Ω, R_1=2MΩ, V_T^-=1.2V, V_T^+=2.2V, $VDDS$=4.18V, is obtained H=1.01496, Fig.16 shows experimental data for Multiple-Sensor Interface with various resistance values connected as the sensor and also shows the plot of $R_{sensor}(f)$ using (15) with the mentioned values of C_1, C_2, R_2, R_1, H.

3.2.3 Multiple-Sensor Interface for capacitive sensors

In case you connect a capacitive sensor (or resistive) to the Multiple-Sensor Interface it will not be able to satisfy the conditions for oscillation of the Pierce oscillator, equations (3) and (4), by $A(\omega_0)\beta(\omega_0)$=1, and so it is again a Schmitt-Trigger relaxation oscillator. So to analyze this circuit the Schmitt-trigger inverter was replaced by a theoretical switch (Schmitt-Trigger), just like previously with resistive sensors.

So the circuit of Fig.17 was analyzed to obtain $f(C_s)$, and then its inverse function $C_s(f)$=C_{sensor} that is useful for using/configuring the Multiple-Sensor Interface. Notice that $i_i \approx 0$ since v_i is the input of the Schmitt-trigger inverter(high-

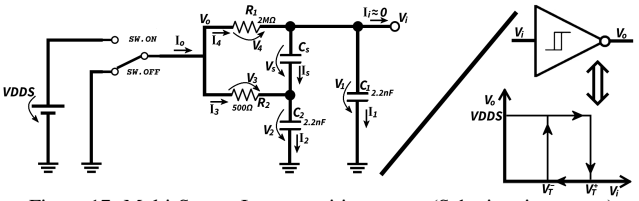

Figure 17: Multi-Sensor Int., capacitive sensor (Schmitt-trigger osc.)

speed Si-gate CMOS) that has a very high input impedance and so $i_i \approx 0$ is an appropriate approximation simplifying the circuit. So from the circuit are obtained the equations:

Nodes and loops: $i_4 = i_s + i_1$, $i_3 + i_s = i_2$, $i_o = i_3 + i_4$, $i_1 + i_2 = i_o$, $i_1 + i_2 = i_3 + i_4$, $v_1 - v_2 - v_s = 0$, $v_4 + v_s + v_2 - v_o = 0$, $v_4 + v_s - v_3 = 0$, $v_3 = v_o - v_2$, $v_4 = v_o - v_i$, $v_2 = v_i - v_s$.

Components: $i_1 = C_1(dv_1/dt)$, $i_2 = C_2(dv_2/dt)$, $v_3 = R_2 i_3$, $v_4 = R_1 i_4$, $i_s = C_s(dv_s/dt)$.

Solving:

$$\frac{v_o - v_i}{R_1} = C_s\frac{dv_s}{dt} + C_1\frac{dv_i}{dt} \tag{16}$$

$$\frac{v_o - v_2}{R_2} + C_s\frac{dv_s}{dt} = C_2\frac{dv_2}{dt} \tag{17}$$

$$\frac{v_o - v_2}{R_2} + \frac{v_o - v_i}{R_1} = C_1\frac{dv_i}{dt} + C_2\frac{dv_2}{dt} \tag{18}$$

Since $v_s = v_i - v_2$ then $dv_s/dt = (dv_i/dt) - (dv_2/dt)$, and so using it on equation (16), is obtained:

$$\frac{dv_2}{dt} = \left(1 + \frac{C_1}{C_s}\right)\frac{dv_i}{dt} - \frac{v_o - v_i}{C_s R_1} \tag{19}$$

Using $dv_s/dt = (dv_i/dt) - (dv_2/dt)$ and (19) on equation (17), is obtained:

$$v_2 = v_o + \frac{R_2(C_2+C_s)(v_o - v_i)}{C_s R_1} + R_2 C_s\left(1 - \left(1 + \frac{C_2}{C_s}\right)\left(1 + \frac{C_1}{C_s}\right)\right)\frac{dv_i}{dt} \tag{20}$$

Calculating the derivative of (20) is obtained:

$$\frac{d(v_2)}{dt} = -\frac{R_2(C_2+C_s)}{C_s R_1}\frac{dv_i}{dt} + R_2 C_s\left(1 - \left(1 + \frac{C_2}{C_s}\right)\left(1 + \frac{C_1}{C_s}\right)\right)\frac{d^2 v_i}{dt^2} \tag{21}$$

Now using (20) and (21) to remove the variables v_2 and dv_2/dt from the equation (18), is obtained an equation solvable for determining $v_i(t)$:

$$v_o - v_i = (R_2(C_2+C_s) + R_1(C_1+C_s))\frac{dv_i}{dt} + R_2 R_1(C_1 C_2 + C_s(C_1+C_2))\frac{d^2 v_i}{dt^2} \tag{22}$$

The equation (22) is of the type: $c(v_o - v_i) = b(dv_i/dt) + a(d^2 v_i/dt^2)$, that has the general solution: $v_i(t) = v_o + k_1 e^{\lambda_1 t} + k_2 e^{\lambda_2 t}$, where k_1,k_2 are integration constants to be defined by 'initial conditions' and λ_1, λ_2 are defined by: $a\lambda^2 + b\lambda + c = 0 \Leftrightarrow \lambda = \frac{-b \pm \sqrt{b^2 - 4ac}}{2a}$ and e is the Euler-Napier constant $e = \sum_{n=0}^{\infty}(1/(n!))$.

So for a solution to this circuit: $c = 1$,
$b = (R_2(C_2 + C_s) + R_1(C_1 + C_s))$,
$a = R_2 R_1(C_1 C_2 + C_s(C_1 + C_2))$.

Is selected the solution $\lambda_2 = \frac{-b + \sqrt{b^2 - 4ac}}{2a}$ by setting k_1=0, because is the one that provides an adequate value for $v_i(t)$, $f(C_s)$, consistent with experimental data, however for obtaining the function $C_s(f)$ you may use any.

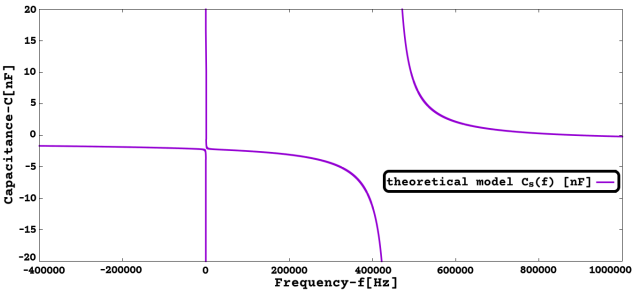

Figure 18: $C_s(f)$ [nF] versus frequency[-400kHz, 1MHz] (Schmitt-Trigger Oscillator, Multiple-Sensor Interface with capacitive sensor).

For convenience of making $v_i(t)$ more similar to typical RC circuits is defined $\tau = -1/\lambda$, and so $v_i(t) = v_o + k_2 e^{-t/\tau_2}$.

So when is connected a capacitive sensor (C_s) the differential equation and solution $v_i(t)$ are the same as when is connected a resistive sensor (R_s), the only differences are on the values of a, b, c; and as such the equations of f(frequency) and T(period) are also the same and are reused from the previous section.

The constant 'H' defined by:

$$H = ln\left(\frac{(V_T^- - VDDS)V_T^+}{(V_T^+ - VDDS)V_T^-}\right),$$

and $f = 1/T \Leftrightarrow f = 1/(\tau_2 H) \Leftrightarrow f = -\lambda_2/H$.

- So the expression (theoretical) of measured capacitance C_{sensor} as a function of frequency(f) is:

$$C_{sensor} = C_s = \frac{(C_1 R_1 + C_2 R_2)Hf - 1 - C_1 C_2 R_1 R_2 H^2 f^2}{Hf((C_1 + C_2)R_1 R_2 Hf - R_1 - R_2)} \tag{23}$$

Using the values C_1=C_2=2.2nF, R_2=500Ω, R_1=2$M\Omega$, V_T^-=1.2V, V_T^+=2.2V, $VDDS$=4.18V, is obtained H=1.01496, Fig.18 shows the plot of $C_s(f)$ using (23) with the mentioned values of C_1, C_2, R_2, R_1, H.

Analyzing the plot on Fig.18 by firstly looking at plot regions with C_s>0, its visible that the $C_s(f)$ plot is over the vertical axis (f=0) and this would mean that for all values of C_s the frequency would be zero (f=0), but visible to the right is another curve that is also placed on the area of C_s>0

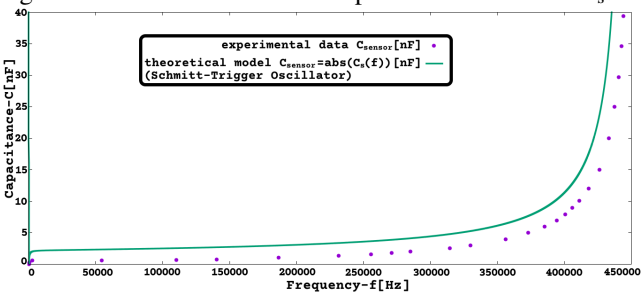

Figure 19: C_s[nF] versus frequency[0Hz, 450kHz] by $|C_s(f)|$ (Schmitt-Trigger osc., Multi-Sensor with capacitive sensor)

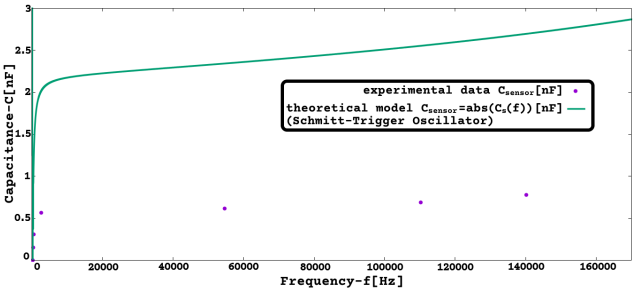

Figure 20: C_s[nF] versus frequency[0Hz, 170kHz] by $|C_s(f)|$ (Schmitt-Trigger osc., Multi-Sensor with capacitive sensor)

(for frequency[447957Hz, 895689Hz]) and at a first view this curve would seem appropriate. But strangely on C_s>0, f>0 for each value of C_s are 2 values of frequency, while for C_s<0, f>0 each value of C_s has only one possible value of frequency (f<0 is considered meaningless/ignored).

The experimental data shows that the way the oscillator works using a capacitive sensor is different from what some would expect on a first view of the plot $C_s(f)$, in order to compare the experimental data with the theoretical model is shown on Fig.19 and Fig.20 the experimental data for Multiple-Sensor Interface with various capacitance values connected as the sensor and also the plot of $abs(C_s(f))$ $(=|C_s(f)|)$ using (23) with the mentioned values of C_1, C_2, R_1, R_2, H.

So it seems that the obtained function of $C_s(f)$ although strangely indicates negative values for the sensor capacitance it can provide a theoretical curve/plot similar to what was obtained on the experimental data for C_{sensor}. On the following sections is given a better insight on why $C_s(f)$ has a negative value.

3.2.4 Multiple-Sensor Int. for measuring frequency

For measuring frequency of an external voltage signal (between 0V and VDDS, so preferentially a digital signal or in case of analog signal it should be limited/trimmed before) is possible to use the mentioned Multiple-Sensor Interface and so using the same port/connector of the device. For this the user should remove/open the jumpers "JP.A", "JP.B" making the capacitors C1-A, C2-B active on the circuit, this will make $C_1 = C_2 = 21.8pF$ that is a quite low capacitance that will have an insignificant effect on the external voltage signal. The external voltage signal should be connected to the 1st pin of the sensor channel that is the one connected directly to input of the Schmitt-Trigger Inverter, so making the inverter directly driven by the external voltage signal, then the Multiple-Sensor Interface is just a converter of the voltage signal to a square wave signal where its frequency will be measured through the counter/timer of the PIC18F2550.

The external voltage signal would preferentially be from a sensor with a square wave output, and the sensor have its power supplied by one of the VDDS,GND ports/connectors of the sensor interface device or by an external connection to the same power supply used to power the device.

3.3 Alternative Approximate Circuit Analysis

3.3.1 Sensor interface circuit simplified

The Multiple-Sensor Interface circuit when working as Schmitt-Trigger oscillator (using R_s, C_s, or L_s with specific C_1,C_2 values) can be studied and understood in a more intuitive way by making some simplification/approximation that may be inaccurate for quantitative purposes but still captures its essence, with the benefit of exposing how it works and resulting in much simpler differential equations. So the interface circuit is a more complex Schmitt-Trigger oscillator, but its essence is the same, it is just some capacitors being charged by currents that pass trough some resistors, and the voltage on a capacitor(v_i) will trigger(at V_T^- or V_T^+) a switch(electronic inverter) to change the voltage(v_o) [3] .

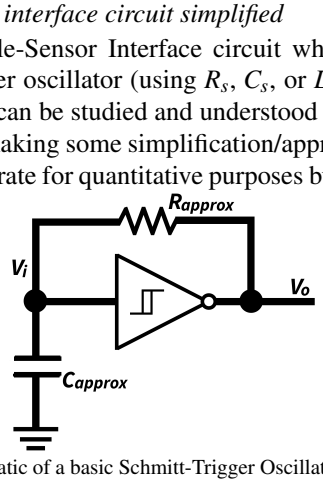

Figure 21: Schematic of a basic Schmitt-Trigger Oscillator to be used as an approximation of the circuit of Multiple-Sensor Interface

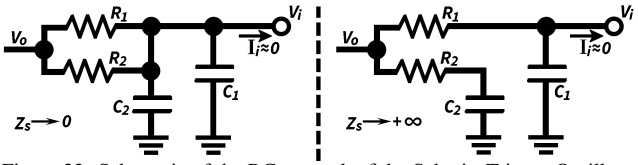

Figure 22: Schematic of the RC network of the Schmitt-Trigger Oscillator for the 2 extreme cases of sensor impedance (Z_s).

So the sensor and interface circuit can be described approximately as a basic Schmitt-Trigger oscillator that only has one capacitor and one resistor (that determine the frequency of oscillation), and so was used the simplified circuit on Fig.21 where C_{approx} is a capacitor and R_{approx} is a resistor that approximate in overall the capacitance and resistance of the sensor interface oscillator.

To build expressions of C_{approx} and R_{approx} that include R_1, R_2, C_1, C_2 are considered initially 2 extreme cases of the sensor impedance(Z_s): 1st $|Z_s|$=0 the sensor can be replaced by a wire, and 2nd $|Z_s|$=∞ the sensor can be removed(open circuit), these 2 extreme cases possible for the sensor impedance are represented on Fig.22 .

Now the sensor can be described as an electric connection that can be weakened or intensified depending on the sensor impedance, so when $|Z_s|$ changes progressively from 0 to $+\infty$ the circuit behavior changes progressively and smoothly from the behavior of the left circuit to the behavior of right circuit of Fig.22. So to obtain equations for R_{approx} and C_{approx} was selected an expression that allows to change smoothly the resistance and capacitance of the left side circuit to the resistance and capacitance of the right side circuit of Fig.22.

So as on Fig.22, here are the values of C_{approx} and R_{approx} for the 2 extreme values of $|Z_s|$=0 and $|Z_s|$=+∞:
$C_{approx}(Z_s=0)=C_1+C_2$; $C_{approx}(Z_s=\infty)=C_1$;
$R_{approx}(Z_s=0)=(R_1R_2)/(R_1+R_2)$; $R_{approx}(Z_s=\infty)=R_1$;

3.3.2 R_{approx} and C_{approx} for a resisitve sensor (R_s)

Here are functions modeled to describe C_{approx} and R_{approx} (with resistive sensor) with a smooth transition from its values at $|Z_s|$=0 and $|Z_s|=+\infty$, where $|Z_s|=R_s$:

$$C_{approx} = (C_1+C_2)\frac{R_1}{|Z_s|+R_1} + C_1\frac{|Z_s|}{|Z_s|+R_1} \tag{24}$$

$$R_{approx} = \frac{R_1R_2}{R_1+R_2}\frac{2R_1}{|Z_s|+2R_1} + R_1\frac{|Z_s|}{|Z_s|+2R_1} \tag{25}$$

Using the equations: $f=1/T \Leftrightarrow f=1/(\tau H) \Leftrightarrow f=-\lambda/H$, and using $\tau=R_{approx}C_{approx}$, where $|Z_s|$ was removed using $|Z_s|=R_s$, it can be obtained $R_s(f)$.

Using values V_T^-=1.2V, V_T^+=2.2V, $VDDS$=4.18V, is obtained H=1.01496 (valid for any type of sensor).

Using the values C_1=C_2=2.2nF, R_2=500Ω, R_1=2MΩ, H=1.01496 with the approximate model (C_{approx}, R_{approx}), is obtained the plot of $R_s(f)$ on Fig.23.

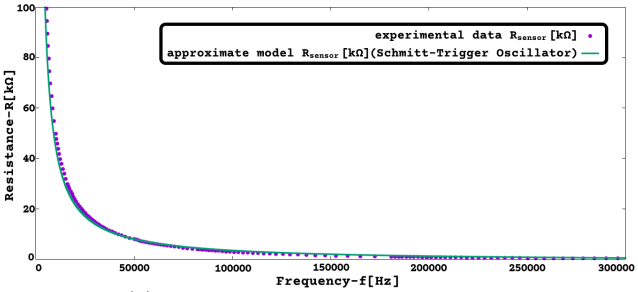

Figure 23: $R_s(f)$[kΩ] by approximate model (C_{approx}, R_{approx}; Multi-Sensor Int. with resistive sensor).

3.3.3 R_{approx} and C_{approx} for an inductive sensor (L_s)

This approximate model for the interface circuit with inductive sensor is only valid for jumper configuration(capacitor values) that make it work as Schmitt-Trigger oscillator, as is expected for JP.A closed, JP.B open (C_1=2.2nF, C_2=21.78pF). Here are functions modeled to describe C_{approx} and R_{approx} (with inductive sensor) with a smooth transition from its values at $|Z_s|$=0 and $|Z_s|=+\infty$, where $|Z_s|=2\pi f L_s$:

$$C_{approx} = (C_1 + C_2)\frac{R_1}{|Z_s|+R_1} + C_1\frac{|Z_s|}{|Z_s|+R_1} \tag{26}$$

$$R_{approx} = \frac{R_1 R_2}{R_1+R_2}\frac{R_1}{|Z_s|+R_1} + R_1\frac{|Z_s|}{|Z_s|+R_1} \tag{27}$$

Using the values C_1=2.2nF, C_2=21.78pF, R_2=500Ω, R_1=2$M\Omega$, H=1.01496 with the approximate model (C_{approx}, R_{approx}), is obtained the plot of $L_s(f)$ on Fig.24 and Fig.25.

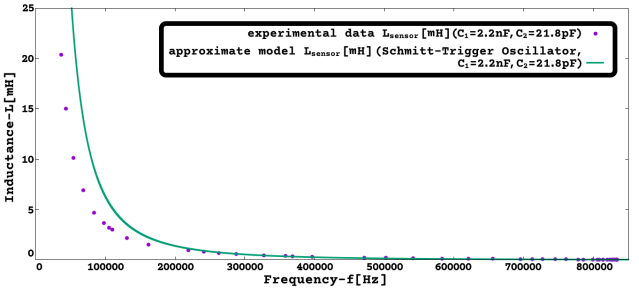

Figure 24: L_s[mH] versus frequency[0Hz, 850kHz] by approximate model (C_{approx}, R_{approx}; Multi-Sensor Int. with inductive sensor)

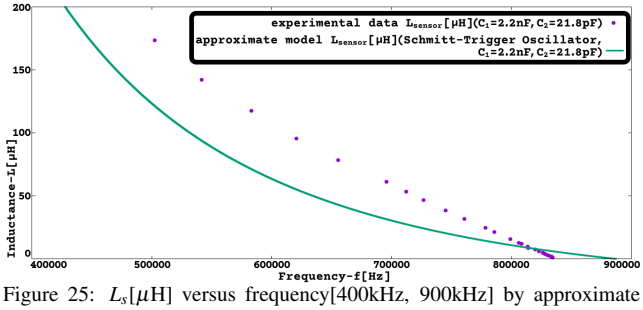

Figure 25: L_s[μH] versus frequency[400kHz, 900kHz] by approximate model (C_{approx}, R_{approx}; Multi-Sensor Int. with inductive sensor)

3.3.4 R_{approx} and C_{approx} for a capacitive sensor (C_s)

Here are functions modeled to describe C_{approx} and R_{approx} (with capacitive sensor) with a smooth transition from its values at $|Z_s|$=0 and $|Z_s|=+\infty$, where $|Z_s|=1/(2\pi f C_s)$:

$$C_{approx} = (C_1 + C_2)\frac{R_1}{|Z_s|+R_1} + C_1\frac{|Z_s|}{|Z_s|+R_1} \tag{28}$$

$$R_{approx} = \frac{R_1 R_2}{R_1+R_2}\frac{R_1}{|Z_s|+R_1} + R_1\frac{|Z_s|}{|Z_s|+R_1} \tag{29}$$

Using the values C_1=C_2=2.2nF, R_2=500Ω, R_1=2$M\Omega$, H=1.01496, with the approximate model (C_{approx}, R_{approx}), is obtained the plot $C_s(f)$ on Fig.26 and Fig.27.

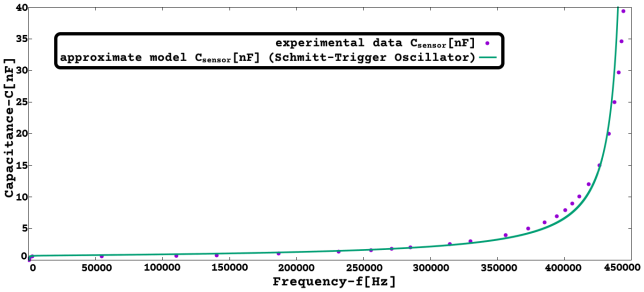

Figure 26: C_s[nF] versus frequency[0Hz, 450kHz] by approximate model (C_{approx}, R_{approx}; Multi-Sensor Int. with capacitive sensor)

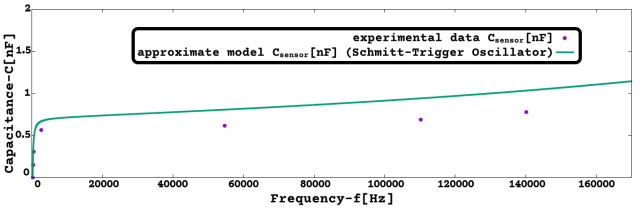

Figure 27: C_s[nF] versus frequency[0Hz, 170kHz] by approximate model (C_{approx}, R_{approx}; Multi-Sensor Int. with capacitive sensor)

4 Discussion

The experimental data obtained when testing the Multiple-Sensor Interface is in overall close to the values calculated using the formulas obtained from the circuit analysis, as it is visible on the various figures that show the plots of the experimental data along with graphs done using the mentioned formulas. In some graphs occurred a deviance or offset between the theoretical and experimental quantitative values, however the observable deviations are not reason for concern as they never affected the similitude between theoretical and experimental graphs (with exception of Fig.13 and Fig.14 that as explained, when using that specific configuration the device no longer behaves as Pierce oscillator, but instead as a Schmitt Trigger oscillator, as it was shown on later subsection using an 'Alternative Approximate Circuit Analysis'). The information that is made available on the article, besides explaining how the device works, may also be useful for a user of the device/technology for determining if a specific sensor of his interest is compatible/usable when connected to the Multiple-Sensor device, namely by observing on the graphs (or tables), for what range of values (min. and max.) of the sensor electrical quantity (R_s or C_s or L_s) it is verified that a change on the quantity the sensor is measuring will produce/cause also a significant or measurable change of the signal frequency on the output of the oscillator used for sensor interfacing.

4.1 Future Work

Further work related to the content/topic and the sensor interface circuit could be developing a better understanding/prediction of why/when the Multiple-Sensor Interface with inductive sensor changes from working as Pierce Oscillator to Schmitt-Trigger Oscillator depending on the values of C_1 and C_2 capacitors (whose values can be adjusted by

jumpers JP.a and JP.B). Also the Multiple-Sensor Interface with inductive sensor as Schmitt-Trigger Oscillator was only analyzed using the approximate model, however it should be possible to obtain $L_s(f)$ (as Schmitt-Trigger Oscillator) using transient circuit analysis, just like it was done for resistive sensor and capacitive sensor.

Other future work, outside the scope of this article, could be characterizing, testing, and comparing this sensor interface circuit for specific sensor types and/or applications, thus allowing a performance comparison with other technologies on specific use cases.

4.2 Why $C_s(f)<0$ on Multi-Sensor with capacitive sensor

About C_s(f)<0 have in mind the Multiple-Sensor with capacitive sensor is studied on transient behavior (relaxation oscillator), where 'frequency' is a measure of the speed of charge and discharge on C1; and also of how fast the transient circuit analysis alternates between v_o=$VDDS$ and v_o=0.

To understand why a normal capacitor behaves as a negative capacitance when connected as the sensor of the Multiple-Sensor Interface (this is, why $C_s(f)<0$), is important to highlight some things already explored on the previous sections:

1) C_1=C_2, $R_1 \gg R_2$.

2) The primary path (always available) to charge C_1 is through R_1, the primary path (always available) to charge C_2 is through R_2, since $R_1 \gg R_2$ and C_1=C_2 this implies that capacitor C_2 will charge/discharge much faster(takes less time) than capacitor C_1.

3) The purpose of sensor C_s on this circuit is to act as a variable impedance that can establish an alternative path on the circuit ($V_o \rightarrow R_2 \rightarrow C_s \rightarrow C_1$) to charge/discharge capacitor C_1; so $C_s \nearrow \Rightarrow |Z_s| \searrow \Rightarrow R_{approx} \searrow \Rightarrow \tau_2 \searrow \Rightarrow$ C_1charges faster.

4) No matter how small $|Z_s|$ may be the capacitor C_2 will always charge/discharge faster than capacitor C_1, and on the limit where $|Z_s|$=0 the capacitors C_1 and C_2 will be charged/discharged simultaneously.

For the following discussion was used as definition of capacitance the formula $C_s = i_s/(dv_s/dt)$, where the $|C_s| = |Q_s|/|v_s|$ (C_s: [F] farad; Q_s: [C] coulomb; v_s: [V] volt), and since the only purpose is to show how C_s can be a negative number it was used the approximate expression $C_s \approx \overline{i_s}/(\Delta v_s/\Delta t)$ that provides exactly the same sign as the exact formula. To show is possible C_s<0 were considered qualitative relations of the circuit electrical parameters on the RC network of the oscillator, the relevant electrical parameters and their variation between t=t_1 and t=t_2 is represented on Fig.28.

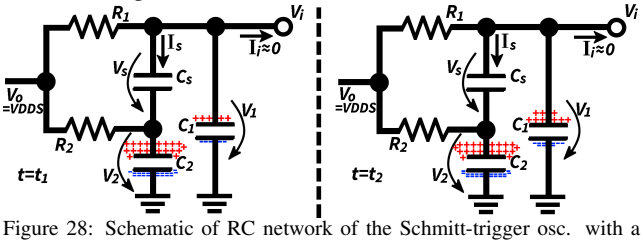

Figure 28: Schematic of RC network of the Schmitt-trigger osc. with a representation of electrical charge on C_1, C_2 on t=t_1 and t=t_2.

It were assumed symbolic values for the voltages on the circuit, used as specimen values to determine how fast a voltage is changing between t_1 and t_2 time moments. So for representing a small amount of electrical charge are used the symbols: [+] for positive charge and [-] for negative charge, since already stated $C_1 = C_2$ for each additional amount of [+] and [-] charge stored on each plate (of C_1 or C_2) will cause an increase of capacitor voltage that will be represented as $[+\underline{v}]$, where $C_1 = C_2 = [+]/[+\underline{v}]$.

As visible on Fig.28, V_o=$VDDS$≈+4.18V, and so $VDDS$ will eventually be the voltage on C_1 and C_2 when t→∞. For making visual on the schematic the charging process, the charge accumulated in C_1, C_2 was divided in 20 sets, each represented by [+], [-]; and for each set of accumulated charge is associated a corresponding increase in voltage of $[+\underline{v}]$, and so $[+\underline{v}] = VDDS/20$.

Accordingly on Fig.28 is represented that C_2 is charged to near the final value ($VDDS$) during the interval $[0;t_1]$ while C_1 charges much slower. During interval $[t_1;t_2]$ is visible that C_2 increased its charge only by 1[+] becoming charged to approximately(or practically) its final value($v_2 \approx VDDS$), whether C_1 is still charging and v_1 is far from its final value($VDDS$), but interestingly v_1 is now increasing faster than v_2, because v_2 already reached its final value, this is $dv_1/dt > dv_2/dt, \forall t \in [t_1;t_2]$. The specimen values here mentioned are in line with the exponential function typical of capacitors charging through a resistor, where lets say a capacitor initially charges very fast, when has some charge stored it charges more slowly, and when close to being full it charges very slowly (where full means the capacitor voltage is close to power supply voltage).

4.2.1 Voltage and current specimens for t=t_1

So looking at the schematic on left side of Fig.28 is visible C_1 and C_2 are charging and for t=t_1 the charge on C_1 is 5[+] and on C_2 is 19[+], so capacitor C_2 is almost charged while C_1 is still charging. Capacitor C_1 is charging through the path $V_o \rightarrow R_1 \rightarrow C_1$ but mainly is charging through path $V_o \rightarrow R_2 \rightarrow C_s \rightarrow C_1$, since $v_2 > v_1$ then $i_s(t=t_1) < 0$.
For t=t_1, Q_1=5[+], Q_2=19[+], then v_1=5$[+\underline{v}]$, v_2=19$[+\underline{v}]$, since v_s=v_1−v_2 then $v_s(t=t_1)$=5$[+\underline{v}]$−19$[+\underline{v}]$=−14$[+\underline{v}]$.

4.2.2 Voltage and current specimens for t=t_2

So looking at the schematic on right side of Fig.28 is visible C_1 and C_2 are charging and for t=t_2 the charge on C_1 is 9[+] and on C_2 is 20[+], so capacitor C_2 is fully charged while C_1 is still charging. Capacitor C_1 is charging through the path $V_o \rightarrow R_1 \rightarrow C_1$ but mainly is charging through path $V_o \rightarrow R_2 \rightarrow C_s \rightarrow C_1$, since $v_2 > v_1$ then $i_s(t=t_2) < 0$.

For t=t_2, Q_1=9[+], Q_2=20[+], then v_1=9$[+\underline{v}]$, v_2=20$[+\underline{v}]$, since v_s=v_1−v_2 then $v_s(t=t_2)$=9$[+\underline{v}]$−20$[+\underline{v}]$=−11$[+\underline{v}]$.

4.2.3 Sign of C_s as calculated from v_s and i_s during $[t_1;t_2]$

The schematics on Fig.28 refer to a charging cycle of the Schmitt Trigger Oscillator. Also $t_2 > t_1 \rightarrow \Delta t > 0$.

For $t \in [t_1;t_2]$ the capacitor C_1 is being charged through the path $V_o \rightarrow R_2 \rightarrow C_s \rightarrow C_1$ and so $i_s(t) < 0, \forall t \in [t_1;t_2] \Rightarrow \overline{i_s} < 0$. Also Δv_s between t_1 and t_2 is Δv_s=$v_s(t=t_2)$−$v_s(t=t_1)$ = −11$[+\underline{v}]$−(−14$[+\underline{v}]$)=3$[+\underline{v}]$, so $\Delta v_s > 0$ between t_1 and t_2.

So concluding between t_1 and t_2, $\Delta t > 0$, $\Delta v_s > 0$, $\overline{i_s} < 0$ $\Rightarrow C_s < 0$ accordingly with $C_s \approx \overline{i_s}/(\Delta v_s/\Delta t)$.

4.3 Comparison to known cases of negative capacitance

Aspects of Multiple Sensor Interface circuit possibly related to negative capacitance phenomenon:
1- Use of Schmitt-Trigger 'NOT' gate which exhibits hysteresis on its $v_o(v_i)$ graph.
2- Multiple Sensor Interface with a capacitive sensor operates under transient(time domain) step voltage changes, caused by its 'NOT' gate(Schmitt-Trigger) alternating between 0V and +VDDS (relaxation oscillator).

Negative capacitance phenomenon is reported on some scientific articles/texts, and interestingly with some coincidence to the 2 aspects mentioned above. Quotes:
1- "Effective negative capacitance has been postulated in ferroelectrics because there is hysteresis in plots of polarization-electric field.", article "Towards steep slope MOSFETs using ferroelectric negative capacitance", by A. O'Neill, year 2014 [4].
2- "The phenomenon of negative capacitance, which has been reported in a variety of situations involving electrolytic as well as electronic systems, ... It is suggested that the physically correct approach lies in the analysis of the corresponding time-domain behavior under step function bias, which involves a current initially falling and then rising gradually over a period of time before finally decaying to zero.", article "The physical origin of negative capacitance", by A. K. Jonscher, year 1986 [5].

5 Conclusions

The author demonstrated theoretically a more versatile design for use with sensor applications, also was provided experimental data that corroborates the presented theory. The motivation of the author was to make available an electronics design that could be more sustainable in terms of life-cycle duration, by making a design more customizable by the user and also not closed/locked to a specific application/purpose. No warranty is given that the design can provide accuracy or convenience to a specific application/use; as the article is focused on showing how a versatile design can be achieved.

Conflicts of interest

The author declares no conflict of interest.

Acknowledgments

I thank all of the Open-Source community for making available technology that everyone can use and build-on freely, thus inspiring me to also release this project as Open-Source. Also thanks to GNUplot software, that was used for drawing the plots on this article [13] .

Appendix A. Experimental Datasets

Experimental data obtained (Fig.5) by using fixed value components connected as the sensor on the device. Were used arrays(PCBs) with inductors, resistors, capacitors that allow to obtain various different values just by changing a jumper/switch, and also single components (including in series or parallel association).

A.1 Frequency measurement by Multi-Sensor

The Multiple-Sensor device measures frequency using a counter inside the microcontroller and has some accuracy and range limitations, it can measure up to 3MHz (higher frequency causes counter overflow). The Multiple-Sensor device was tested with a square wave signal from the signal generator JDS6600 (by Joy-IT, frequency accuracy: ±20ppm).

The Multiple-Sensor device measurement accuracy (percentage error) of frequency, is worst at low frequencies with 9% error at 100Hz and 0.7% error at 1kHz, above 5kHz the error was always smaller than 0.2% (ignoring any accuracy error by JDS6600 used as reference). The Multiple-Sensor device measurement precision (variation) for frequency was worst at low frequencies with 5% variation at 300Hz, above 1500Hz was always smaller than 1%, and above 15kHz was always smaller than 0.1%.

A.2 Experimental data on Multi-Sensor Int

- Reference instruments:
The measurements of inductance(L_s) and capacitance(C_s) were obtained using the LCR meter TH2821A (by Tonghui, basic accuracy 0.3%), configured to 10Khz test signal.

The measurements of resistance(R_s) were obtained using the meter UT603 (by UNI-T, accuracy: 0.8% for R≤2MΩ; 2% for R>2MΩ).

- Jumper Configurations:

[a](JPA on, JPB off): C_1=2.2nF; C_2=21.8pF.
[b](JPA off, JPB on): C_1=21.8pF; C_2=2.2nF.
[c](JPA on, JPB on): C_1=2.2nF; C_2=2.2nF .

- Units: Hz=hertz, H=henry, Ω=ohm, F=farad.

Here is made available, the sets of experimental data that were used for drawing the plots of $L_s(f)$, $R_s(f)$, $C_s(f)$, these are the measured values of inductance, resistance, capacitance paired with measured frequency on the Multiple Sensor Interface device.

Table 2: Set of experimental data for $C_s(f)$

C_s[nF] Capacitance	f[Hz][c] JPA on, JPB on	C_s[nF] Capacitance	f[Hz][c] JPA on, JPB on
0	229	4.97	373045
0.152	321	5.97	385032
0.31	458	6.95	394283
0.568	2614	7.94	400750
0.615	54570	8.98	405766
0.689	110286	10.07	411246
0.776	140178	12.04	418028
1.015	186522	15.02	426040
1.34	231460	20.02	433089
1.58	255526	24.97	437446
1.79	271015	29.68	440382
2	285020	34.62	442584
2.56	314530	39.43	444235
2.99	329820	44.38	445688
3.98	356012	49.38	446712

Precision error(maximum frequency variation):
±3kHz (600pF<C_s<1.6nF);
±2kHz (1.6nF<C_s<21nF);
±1kHz (C_s>21nF); ±50Hz (C_s<600pF).

Table 3: Set of experimental data for $L_s(f)$

$L_s[\mu H]$ Inductance	f[Hz][a] JPA on, JPB off	f[Hz][b] JPA off, JPB on	f[Hz][c] JPA on, JPB on
1.21	834161	879205	446590
1.4	833855	885138	476589
1.65	833350	888501	473393
1.85	833014	887049	458577
2.51	831302	881055	494096
3.09	829880	892844	474739
3.8	828045	898700	467354
4.1	827433	891116	466711
4.7	826011	881239	496405
5.87	823121	873380	519263
7.32	819681	915412	577595
8.76	813947	864236	591646
9.7	813397	858548	615743
11.77	808321	936894	1432920
12.84	805905	934723	1357220
15.76	799009	895932	1251070
21.39	785691	931940	1090760
24.49	778123	978330	1011830
31.8	760632	1056660	889633
38.61	745112	1193360	809559
46.7	726580	1369450	736014
53.44	712070	2853370	690970
61.3	695603	2662840	639014
78.3	655604	2332760	568099
95.34	620697	2103380	509845
117.6	583023	1899190	464617
142.28	541388	1722220	420062
173.5	502398	1575330	382571
201.5	471222	1464370	354070
271.46	396546	1201810	292482
341.8	368641	1112820	271168
360.6	357938	1085180	261856
438.7	327053	994721	239762
558.1	287880	868105	212362
660.7	262804	794697	194290
777.6	241031	737803	178480
921.2	218738	677591	163587
1491	161768	606844	124338
2171	130897	499264	102978
2976	109912	446452	87856
3170	105439	406011	84614
3640	97779	383305	79110
4646	84110	319423	69783
6880	68162	282360	57750
10140	54034	224090	47230
15040	43377	192088	38790
20375	36588	171981	33683

Precision error(maximum frequency variation):
$\pm$2kHz (at high 'f[Hz]'); $\pm$300Hz (at low 'f[Hz]');
$\pm$5kHz (2.85MHz$\leftrightarrow$1.36MHz; at [b] JPA off, JPB on).

Table 4: Set of experimental data for $R_s(f)$

$R_s[\Omega]$ Resistance	f[Hz]^c JPA on, JPB on	$R_s[\Omega]$ Resistance	f[Hz]^c JPA on, JPB on	$R_s[\Omega]$ Resistance	f[Hz]^c JPA on, JPB on	$R_s[\Omega]$ Resistance	f[Hz]^c JPA on, JPB on
0	456284	577	231735	4180	79553	28900	16666
1.2	454678	597	228447	4380	77107	29900	16176
2.2	453975	617	225252	4580	74783	31900	15244
3.2	453149	637	222178	4780	72612	33900	14418
4.2	452400	657	219228	4980	70593	35900	13669
5.2	451605	677	216353	5180	68682	37800	13027
6.2	450718	697	213647	5380	66863	39800	12430
7.2	449923	717	210971	5580	65135	41800	11880
8.2	449067	736	208402	5770	63514	43800	11375
9.2	448272	756	205910	5970	61985	45800	10917
10.2	447385	776	203464	6170	60517	47800	10488
15.2	443226	796	201139	6370	59111	49800	10091
20.1	439144	816	198877	6570	57765	54800	9235
25.1	435183	836	196659	6770	56511	59800	8531
30.1	431269	856	194504	6970	55288	64800	7904
35.1	427447	876	192409	7170	54126	69700	7385
40	423655	896	190406	7370	53010	74700	6926
45	420016	916	188418	7570	51940	79700	6513
50	416407	936	186476	7760	50915	84600	6146
55	412845	955	184611	7960	49952	89600	5825
60	409359	975	182776	8460	47643	94600	5550
65	406010	996	180865	8960	45548	99400	5320
69.9	402601	1096	172578	9460	43622	109400	4862
74.9	399328	1195	165208	9960	41879	119300	4479
79.9	396209	1295	158603	10460	40243	129300	4158
84.9	393060	1394	152594	10960	38760	139300	3883
89.9	390017	1494	147150	11460	37353	149300	3623
94.8	387005	1593	142135	11960	36053	159200	3440
99.9	383396	1693	137548	12450	34861	169200	3256
119.7	372387	1792	133298	12960	33714	179100	3073
139.7	361700	1892	129353	13450	32659	189100	2935
159.6	351608	1992	125699	13950	31680	199100	2798
179.5	342205	2090	122258	14450	30732	299000	1972
199.5	333306	2190	119017	14950	29861	398000	1544
219	325050	2290	115974	15440	29035	498000	1284
239	317236	2390	113115	15940	28255	597000	1100
259	309836	2490	110409	16440	27522	697000	978
279	302879	2590	107855	16940	26818	796000	886
299	296289	2690	105424	17430	26145	896000	825
319	290112	2790	103115	17930	25503	995000	779
339	284225	2890	100914	18430	24907	1495000	596
359	278614	2990	98819	18930	24326	1993000	504
378	273308	3090	96831	19420	23775	2490000	458
398	268278	3190	94905	19940	23271	3090000	412
418	263462	3290	93070	20900	22292	4080000	366
438	258829	3390	91327	21900	21375	5080000	351
458	254471	3490	89645	22900	20549	6070000	336
478	250251	3580	88024	23900	19769	7070000	321
498	246214	3680	86464	24900	19066	8050000	321
518	242361	3780	84966	25900	18393	9040000	305
538	238646	3880	83529	26900	17782		
557	235144	3980	82153	27900	17201		

Precision error(maximum frequency variation):
$\pm$1kHz(at low R_s); $\pm$300Hz(at 30kΩ); $\pm$100Hz(at high R_s).

References

[1] R.C. Jaeger, T.N. Blalock (2011). Microelectronic Circuit Design (4th ed.). McGraw–Hill. ISBN 978-0-07-338045-2. - "C.2 THE HYBRID OR h-PARAMETERS - Appendix C Two-Port Review" - Pag.1310-1311 . *Alternative Source: "Hybrid parameters (h-parameters) - Two-port Network - Wikipedia (2020)"* - https://en.wikipedia.org/wiki/Two-port_network

[2] Peter McLean (2020). Topic 4 - Crystal Oscillators (Pierce oscillator analysis) - Digital Electronics (UTS-AU). Accessed July 2021. https://pmcl.net.au/de .

[3] Eduardo Corpeno - AllAboutCircuits (2018). Exactly How Schmitt Trigger Oscillators Work. Accessed July 2021. https://www.allaboutcircuits.com/technical-articles/exactly-how-schmitt-trigger-oscillators-work .

[4] A. O'Neill, D. Appleby, N. Ponon, K. Kwa (2015). Towards steep slope MOSFETs using ferroelectric negative capacitance. 2014 12th IEEE International Conference on Solid-State and Integrated Circuit Technology (ICSICT). DOI: 10.1109/ICSICT.2014.7021281 .

[5] Andrew K. Jonscher (1986). The physical origin of negative capacitance. J. Chem. Soc., Faraday Trans. 2, vol. 82, no. 1, Pag.75-81. DOI: 10.1039/F29868200075 .

[6] S. N. Nihtianov, G. P. Shterev, B. Iliev and G. C. M. Meijer, (2001), An interface circuit for R-C impedance sensors with a relaxation oscillator. IEEE Transactions on Instrumentation and Measurement, vol. 50, no. 6, Pag. 1563-1567, DOI: 10.1109/19.982945 .

[7] J. H. Lu, M. Inerowicz, S. Joo, J. Kwon and B. Jung, (2011), A Low-Power, Wide-Dynamic-Range Semi-Digital Universal Sensor Readout Circuit Using Pulsewidth Modulation. IEEE Sensors Journal, vol. 11, no. 5, Pag. 1134-1144. DOI: 10.1109/JSEN.2010.2085430 .

[8] F.M.L.v.d. Goes, G.C.M. Meijer, (1997). A Universal Transducer Interface for Capacitive and Resistive Sensor Elements. Analog Integrated Circuits and Signal Processing 14, Pag. 249–260. DOI: 10.1023/A:1008246103915 .

[9] Xiaowen Liu, D. Rairigh, Chao Yang and A. J. Mason, (2009) Impedance-to-digital converter for sensor array microsystems, 2009 IEEE International Symposium on Circuits and Systems (ISCAS), Pag. 353-356, DOI: 10.1109/ISCAS.2009.5117758 .

[10] Dumbrava V., Svilainis L. (2007). The Automated Complex Impedance Measurement System. Elektronika Ir Elektrotechnika, 76(4), Pag. 59-62. https://eejournal.ktu.lt/index.php/elt/article/view/10720

[11] HIOKI website (2021), LCR meter basic measurement principles. Accessed December 2021. https://www.hioki.com/global/learning/usage/lcr-meters_1.html .

[12] Bi H., Yin K., Xie X., Ji J., Wan S., Sun L., Terrones M., Dresselhaus M. S., (2013). Ultrahigh humidity sensitivity of graphene oxide. Sci Rep. 2013;3:2714. DOI: 10.1038/srep02714 .

[13] Thomas Williams, Colin Kelley (2007) - GNUplot software. Accessed July 2021. http://gnuplot.sourceforge.net .